Microwave Signal Rectification Using Artificial Composite Materials Composed of Diode-Loaded Electrically Small Dipole Antennas

Fabrice Auzanneau and Richard W. Ziolkowski, *Fellow, IEEE*

***Abstract*— The electromagnetic properties of composite materials composed of dipole or loop antennas (also called molecules) loaded with different linear passive electronic circuits are summarized. These molecules are extended to those molecules whose loads contain some basic nonlinear elements. Several examples are discussed. The simplest nonlinear load is the clamping circuit: a diode and a resistor are connected in series to an electrically small dipole antenna. This is generalized to a more complicated molecule based on a diode bridge. Numerical results generated with a finite-difference time-domain (FDTD) simulator demonstrate how an incident narrow-bandwith pulse interacts with these materials and can be transformed into a baseband, rectified signal, or a signal containing selected harmonics of the fundamental frequency. Potential applications of these artificial material-based signal convertors include target identification and signal modulation.**

***Index Terms*— FDTD, harmonics, nonlinear devices, rectification, synthetic materials.**

I. Introduction

THERE ARE many potential applications of artificial dielectric and magnetic materials to microwave engineering. Engineers in their unending quest to improve device and system performances are beginning to utilize a variety of complex materials to increase the degrees of freedom available to them in the design and fabrication processes. Artificial chiral materials [1]–[3] have been studied extensively in recent years in this context in an attempt to realize more efficient radar-absorbing coatings. Metallic helices embedded in dielectric substrates have led to bianisotropic materials with interesting electric and magnetic properties.

We have introduced elsewhere [4]–[8] the concept of constructing materials using artificial molecules formed by electrically small antennas connected to specified passive linear electronic loads. By varying the loads, we have demonstrated that the properties of these materials can be designed for a variety of applications. Traditional material behaviors, the Debye and Lorentz models, as well as their generalizations to include more inclusive polarization and magnetization excitations, the time-derivative Debye, time-derivative Lorentz, two time-derivative Lorentz, etc., models, have been realized in this manner. Numerical simulations have demonstrated their efficacy individually as electrically or magnetically lossy dispersive materials, as well as in matched combinations to form nonreflective absorbers.

With the increase of activity in utilizing active elements in many RF systems [12]–[20], we have been led to the idea of incorporating nonlinear components into the loads which form these artificial molecules. The degrees of freedom in the variations in the behaviors of the individual molecules increase dramatically. Materials could be designed to act as convertors which transform narrow-bandwidth signals into signals with multiple harmonic content or even into baseband signals. However, because they are nonlinear, the loads and resulting small antenna behaviors cannot be realized from a frequency-domain analysis. A full transient characterization of these molecules is necessary. Once the response of an individual molecule is realized, its use in the construction of a composite artificial material can be considered. The behaviors of the composite materials can then be modeled to define their usefulness to a variety of applications.

In Section II of this paper, we summarize our realizations of electric and magnetic molecules, which are based upon linear passive loads. In Section III, we extend this analysis to nonlinearly loaded antennas and achieve an accurate assessment of their behaviors. The finite-difference time-domain (FDTD) method is emphasized throughout. We demonstrate the approach using diode elements in the loads to achieve clamping effects and transform a narrow-bandwidth pulse into a baseband large bandwidth pulse using a slab of this material. The loads are extended to a diode bridge in Section IV. This molecule allows us to create a material which produces time signals containing only the odd harmonics of the incident signal. The FDTD models used to assess these molecules are discussed throughout these sections. We summarize our results in Section V.

II. Antennas

We consider here electrically small loaded dipole antennas, as shown in Fig. 1. The dipole antenna has the half-length

Manuscript received September 17, 1997; revised June 22, 1998. This work was supported in part by the Office of Naval Research under Grant N0014-95-1-0636 and by the Air Force Office of Scientific Research, Air Force Materiel Command (USAF) under Grant F49620-96-1-0039.

F. Auzanneau is with CEA CESTA, 33114 Le Barp, France (e-mail: auzannea@bordeaux. cea.fr).

R. W. Ziolkowski is with the Department of Electrical and Computer Engineering, University of Arizona, Tucson, AZ 85721-0104 USA (e-mail: ziolkows@ece.arizona.edu).

Publisher Item Identifier S 0018-9480(98)08022-3.

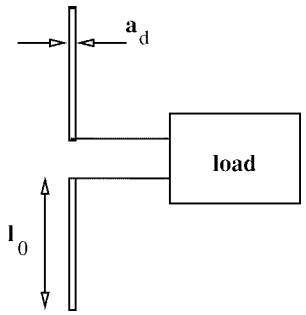

Fig. 1. Basic description of the electrically small loaded dipole antenna.

l_0 and wire diameter a_d. The dipole antenna connected to its load (electronic circuit) is called an "electric molecule." We have derived the properties of several linearly loaded electric molecules in previous papers [4]–[8] simply by using a scheme based on the impedances of the loads. This approach leads to electric susceptibilities χ_e of the following form:

$$\chi_e = \frac{K_e}{-j\omega\left(Z_{\text{in}}^d + Z_L^d\right)} \tag{1}$$

where a $-j\omega t$ convention is understood and omitted throughout. The electric constant K_e depends on the dimensions of the antenna and polarization coupling factors describing the relative orientation of the field components and antenna. The input impedance of the antenna is labeled by Z_{in}^d and the impedance of the load is labeled by Z_L^d. For the electrically small dipole antenna under consideration here, the input impedance is given by

$$Z_{\text{in}}^d = \frac{1}{-j\omega C_d} \tag{2}$$

where the constant $C_d = \pi\epsilon_0 l_0/\ln(4.0l_0/a_d)$ is the equivalent capacitance of the antenna. We also have obtained the corresponding time-domain behavior of these molecules.

We have demonstrated [4]–[8] that with variations of passive linear loads (circuits), one can obtain composite dielectric materials constructed from the resulting single-antenna molecules whose electromagnetic response is described by traditional polarization models such as the following Debye and Lorentz forms [9], [10]:

$$\frac{\partial}{\partial t}\vec{P} + \frac{1}{\tau}\vec{P} = \frac{1}{\tau}\epsilon_0\chi_D\vec{E} \quad \text{(Debye)} \tag{3}$$

$$\frac{\partial^2}{\partial t^2}\vec{P} + \Gamma\frac{\partial}{\partial t}\vec{P} + \omega_0^2\vec{P} = \epsilon_0\omega_0^2\chi_L\vec{E} \quad \text{(Lorentz)} \tag{4}$$

where $\vec{P}$ is the polarization of the molecule, ϵ_0 is the permittivity of vacuum, and the constants χ_D, τ, Γ, ω_0, and χ_L are related to the values of the components in the load circuits and, hence, characterize the particular material model. We have also obtained their generalizations [10], [11], e.g., the time-derivative Debye material (TD-DM), the time-derivative Lorentz material (TD-LM), the two time-derivative Lorentz material (2TD-LM), etc., to include more inclusive polarization behaviors, i.e.,

Model	dipole's load	
Debye	R	
TD Debye	R/C	C/(R-C)
Lorentz	R-L-C	
TD Lorentz	L/R	R-(R/C)
	R-(R/L)	C-(R/L)
	R/(R-C)	
2TD Lorentz	R/L/C	C/(R-L)
	C/(R-L-C)	R/C/(R-L)
	R/C/(R-C)	C-(R/L/C)
TD AZ	L-(R/C)	L-(R/L)
	L/(R-L)	R-L-(R/C)
	R-L-(R/L)	
2TD AZ	R-(L/C)	R/(L-C)
	R-(R/L/C)	R/(R-L-C)
	L/(R-C)	(L-C)/(R-C)
	(R/L)-(R/C)	(R-C)/(R-L)
3TD-AZ	(L/C)-(R/C)	(L/C)-(R/L)
	(R/C)-(R/L/C)	R/C/(L-C)
	R/C/(R-L-C)	
2TD 4^{th} order	L-(R/L/C)	(L-C)/(R-L)
	(L-C)/(R-L-C)	(R-L)/(R-L-C)
	(R-L-C)/(R-L-C)	R-L-(L/C)
	R-L-(R/L/C)	
3TD 4^{th} order	(R/L)-(R/L/C)	(R-C)/(R-L-C)
4TD 4^{th} order	(L/C)-(R/L/C)	(R/L/C)-(R/L/C)
3TD 5^{th} order	L/(R-L-C)	

- $\Longleftrightarrow$ 'in series' — / $\Longleftrightarrow$ 'in parallel'

Fig. 2. Potential constructions of several dielectric-material models from electric molecules with passive linear loads.

$$\frac{\partial}{\partial t}\vec{P} + \frac{1}{\tau}\vec{P} = \frac{1}{\tau}\epsilon_0\chi_\alpha\vec{E} + \epsilon_0\chi_\beta\frac{\partial}{\partial t}\vec{E} \quad \text{(TD-DM)} \tag{5}$$

$$\frac{\partial^2}{\partial t^2}\vec{P} + \Gamma\frac{\partial}{\partial t}\vec{P} + \omega_0^2\vec{P} = \epsilon_0\omega_0^2\chi_\alpha\vec{E} + \epsilon_0\omega_0\chi_\beta\frac{\partial}{\partial t}\vec{E} \quad \text{(TD-LM)} \tag{6}$$

$$\frac{\partial^2}{\partial t^2}\vec{P} + \Gamma\frac{\partial}{\partial t}\vec{P} + \omega_0^2\vec{P} = \epsilon_0\omega_0^2\chi_\alpha\vec{E} + \epsilon_0\omega_0\chi_\beta\frac{\partial}{\partial t}\vec{E} + \epsilon_0\chi_\gamma\frac{\partial^2}{\partial t^2}\vec{E} \quad \text{(2TD-LM).} \tag{7}$$

Molecules can be designed to yield even more complex material behaviors in which three (labeled AZ models) and four (labeled fourth-order models) time derivatives of the polarization are related to multiple time derivatives of the electric fields. The circuit combinations of passive components, which we have determined will yield all of these material characteristics, are listed in Fig. 2.

Since it is based upon an indirect frequency-domain analysis, our previous approach is no longer effective if the loads are nonlinear. We now need to directly derive in the time domain the expressions for the currents at the terminals of the antennas and then determine the electromagnetic field radiated by those currents. The computation of the currents is now possible by solving a set of nonlinear ordinary differential

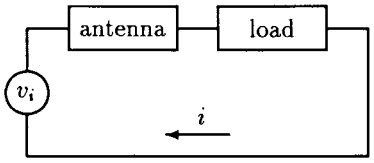

Fig. 3. Thevenin's equivalent circuit for an electric molecule.

equations describing the behavior of the total circuit, including the antenna and load. In the case of the dipole antenna and its load, this modelization is obtained by representing the electric molecule by an equivalent Thevenin's circuit, as shown in Fig. 3.

For the dipole antenna, the current at its terminals i is related to the interacting electric field $\vec{E}$ through the relations

$$\epsilon_0 \frac{\partial}{\partial t}\vec{E} = +\nabla \times \vec{H} - \frac{\partial}{\partial t}\vec{P} \tag{8}$$

$$\frac{\partial}{\partial t}\vec{P} = -\frac{l_0}{V} i\hat{n} \tag{9}$$

where $\vec{P}$ is the effective polarization of the dipole and $\hat{n}$ is the unit vector which represents its orientation. The constant V represents the effective volume associated with each molecule. The source voltage for the circuit is given by the open circuit voltage of the receiving antenna with no load

$$v_i = -l_0 \vec{E} \cdot \hat{n}. \tag{10}$$

As with the linear passive loads, the specification of the passive and active nonlinear loads for the electric molecules will determine the response of the resulting composite dielectric materials. The modeling of the circuit behavior can be readily accomplished with several numerical methods or the SPICE circuit simulation package [12]–[20]. The modeling of the interactions of an electromagnetic field with the composite material can be accomplished with extensions of a FDTD simulator to include the additional time-domain ordinary differential equations that model the circuit voltages and currents.

In the same context, we have also derived the properties of magnetic molecules, which are formed by electrically small loaded loop antennas and the corresponding frequency- and time-domain models of the magnetization fields. In particular, we have emphasized magnetic molecules that are dual to the electric ones to achieve reflectionless absorbers. However, here, we are interested in molecules with nonlinear loads. Loads connected to an electric dipole are nonlinear by virtue of their nonlinear current response to an applied voltage. Circuit devices to achieve the corresponding nonlinear voltage response to an applied current do not exist. This limits our ability to form matched nonlinear materials that could lead to electromagnetic absorbers. Additionally, we have found that the responses of the magnetic molecules that do follow from the nonlinear voltage devices such as the diode are several orders of magnitude smaller than they would be if the corresponding nonlinear current devices did exist. Thus, these magnetic molecules are not pursued further in this paper.

III. Clamping Molecules

The simplest nonlinear circuit is the clamping circuit. The clamping circuit consists of a source driving the load, which is composed of a diode and resistor. Its response prevents the current from becoming more negative than a prescribed saturation current value I_s. The diode is a passive nonlinear element; it is modeled by the following nonlinear expression, which relates the current flowing through it i and, hence, the circuit, to the voltage v_d applied to the diode

$$i(t) = I_s(e^{\alpha v_d(t)} - 1) \tag{11}$$

where the exponential constant $\alpha = q/nkT$ is set to the value $\alpha = 40\ \mathrm{V}^{-1}$ and the amplitude constant I_s is set to the value $I_s = 2.0 \times 10^{-9}\ A = 2.0$ nA for all of the following examples discussed.

A. Clamping Circuit Load for the Electric Dipole

When this clamping load is connected to the electric dipole, we find that in addition to (11), the following equations govern the behavior of this electric molecule:

$$v_i = v_c + v_d + Ri \tag{12}$$

$$\frac{dv_c}{dt} = \frac{i}{C_d} \tag{13}$$

where v_c is the voltage measured across the capacitor.

If we differentiate (11) with respect to time, we obtain

$$\frac{di}{dt} = \alpha \frac{dv_d}{dt}(i + I_s). \tag{14}$$

Combining this relation with the time derivative of the voltage relation (12), we generate the following differential equation, which describes the behavior of the molecule by itself:

$$\frac{di}{dt} = \frac{\alpha(i + I_s)}{1 + R\alpha(i + I_s)}\left(\frac{dv_i}{dt} - \frac{i}{C_d}\right). \tag{15}$$

In the case of a sinusoidal input voltage source ($v_i = V_0 \sin \omega_0 t$), a Runge–Kutta (RK) solver [21] gives the behavior of the diode voltage and current shown in Fig. 4. The clamping effect on the current is clearly visible and the spectrum of the diode current shows that the nonlinear diode creates several new harmonics of the input angular frequency ω_0. The current decay is caused by the charging of the capacitor in the circuit, which only occurs on the positive swings of the voltage. As the capacitor charges, it produces a current that opposes the source current. The decay rate of the current is related to the capacitive charging rate $1/RC_d$.

In order to model the behavior of a composite material composed of these electric clamping molecules, we need to include (15) into our FDTD simulator. In one spatial dimension (x-polarized wave propagating in the $+z$-direction) and time, (8) and (9) lead to the equation set

$$\epsilon_0 \frac{\partial}{\partial t} E_x = -\frac{\partial}{\partial z} H_y - \frac{\partial}{\partial t} P_x \tag{16}$$

$$\frac{\partial}{\partial t} P_x = -\frac{l_0}{V} i. \tag{17}$$

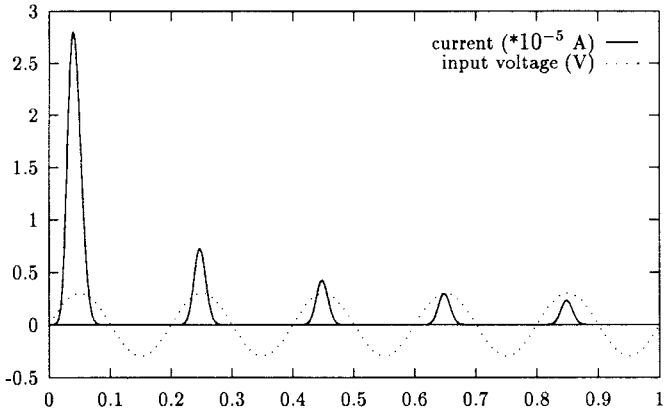

Fig. 4. Clamped electric dipole response: diode current i and incident voltage v_i versus time (nanosecond).

The electric field is related to the source voltage via (10). These relationships lead to the expression

$$\frac{dv_i}{dt} = -l_0 \frac{\partial E_x}{\partial t} = \frac{l_0}{\epsilon_0}\frac{\partial H_y}{\partial z} - \frac{l_0^2}{\epsilon_0 V} i \tag{18}$$

and, hence, to the ordinary differential equation for the current

$$\frac{di}{dt} = \frac{\alpha(i+I_s)}{1+R\alpha(i+I_s)}\left[\frac{l_0}{\epsilon_0}\frac{\partial H_y}{\partial z} - \left(\frac{1}{C_d} + \frac{l_0^2}{\epsilon_0 V}\right) i\right]. \tag{19}$$

In comparison to (13), a new term $(l_0^2/\epsilon_0 V)i$ appears in (19) from the presence of the polarization field in the composite material, which acts as a capacitance with equivalent value $C_s = \epsilon_0 V/l_0^2$ in series with the dipole moment of the individual molecule. Equation (19) is the desired auxiliary nonlinear differential equation describing the behavior of the nonlinear electric molecules in the composite material. Due to the nonlinear form of this expression, we expect that there will be harmonics of the frequency of the incident field present in the spectrum of the scattered field.

Note that substituting the expressions for P_x and v_i [(16) and (18)] into (15) for the current variation in time gives us a constitutive relation $D_x = \epsilon E_x + P_x$ for the composite material, which is quite complicated because the polarization field satisfies the highly nonlinear relation

$$\frac{1}{C_d}\frac{\partial P_x}{\partial t} + \left[R + \frac{1}{\alpha\left(I_s - \frac{V}{l_0}\frac{\partial P_x}{\partial t}\right)}\right]\frac{\partial^2 P_x}{\partial t^2} = \frac{l_0^2}{V}\frac{\partial E_x}{\partial t}. \tag{20}$$

With such a nonlinear relationship, it is readily observed that an accurate description of the material behavior can only be obtained numerically, as described in the following sections.

B. FDTD Results

To simulate and understand the behavior that could arise from a composite material composed of clamped electric molecules, we coupled (19) for the circuit current at each time step and space location in the medium with Maxwell's equations

$$\frac{di}{dt} = \frac{\alpha(i+I_s)}{1+R\alpha(i+I_s)}\left[\frac{l_0}{\epsilon_0}\frac{\partial H_y}{\partial z} - \left(\frac{1}{C_d} + \frac{l_0^2}{\epsilon_0 V}\right) i\right] \tag{21}$$

$$\frac{\partial}{\partial t} H_y = -\frac{1}{\mu_0}\frac{\partial}{\partial z} E_x \tag{22}$$

$$\frac{\partial}{\partial t} E_x = -\frac{1}{\epsilon_0}\frac{\partial}{\partial z} H_y + \frac{l_0}{\epsilon_0 V} i. \tag{23}$$

The electric field was obtained at integer time steps, and the magnetic field at half-integer time steps. The magnetic-field locations are located a half spatial step separated from the electric-field locations. The current was taken to be coincident with the magnetic field in both space and time locations. The magnetic-field (22) and electric-field (23) update equations were solved in the usual leapfrog manner. We used a simple fourth-order RK solver to solve (21) for the current. Since the RK method produces an update value a full time step from the previous value and because (21) also depends on the magnetic field values, the current update was obtained at the next half-integer time step before the magnetic field was updated to that time value. These choices determined the ordering of (21)–(23). We found that we needed to run our solver in double precision on a DEC ALPHA 600 5/333 workstation to minimize the numerical inaccuracies. The Courant stability number $\xi = \Delta t/(c\Delta z)$ was set at $\xi = 0.5$ for the single slab and $\xi = 0.25$ for the following two-slab cases. Running the simulator with $\xi = 1.0$ would cause the integrator to advance too fast in time and miss the nonlinearity in some instances.

A pulsed plane wave was launched from a total field-scattered field boundary. It was incident on a slab of composite material which consisted of a substrate with permittivity ϵ_0 and permeability μ_0 with our clamped electric molecules embedded in it, each molecule being effectively contained within one FDTD cell. Let the normal to the slab be in the $+\hat{z}$-direction, the direction of propagation of the incident plane wave. The dipole is oriented orthogonal to this direction along the electric field ($\hat{x}$-direction). The slab parameters were selected to achieve interesting effects for a unit amplitude incident plane wave. Since only the electric dipole antennas are involved, the effective volume of the molecules was selected to be a cylindrical volume surrounding each of them. To allow us to consider the composite material in a Maxwell–Garnett sense [22], [23], the volume was specified to be 20 times as large as the volume of the antenna, i.e.,

$$V = 20.0 \times \left[\pi\left(\frac{a_d}{2}\right)^2 (2l_0)\right] \tag{24}$$

which gives a 5.0% volume fill-factor for the material. The half-length of the dipole was $l_0 = 5.0$ cm and the wire diameter was $a_d = 0.1382$ mm $= l_0/362$. The value of the resistor was set to be $R = 10.0\ \Omega$ in the runs reported below. We have found the behavior of the clamped molecules varies little from this value of the resistance up to $R = 10.0$ kΩ.

The pulsed incident electric field had the form

$$E^{\text{inc}}(t) = [1-(t/T)^2]^4 \sin(2.0\pi f_{\text{inc}} t) \tag{25}$$

where the driving frequency was set at $f_{\text{inc}} = 1.0$ GHz ($\lambda_{\text{inc}} = 300.0$ mm) and the total pulse length was $T =$

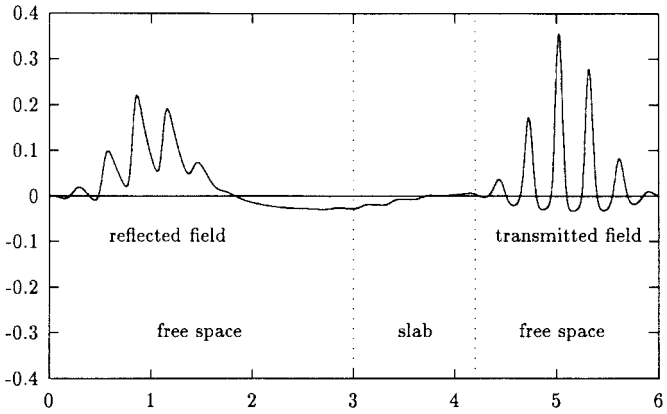

Fig. 5. Scattering from a slab of clamping electric molecules. Electric field (volt per meter) versus simulation region distance (meter).

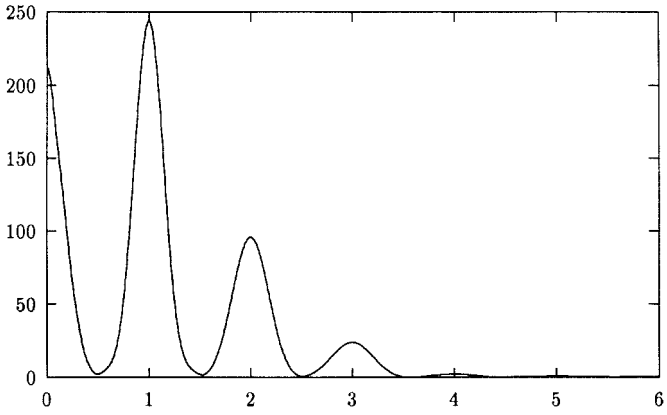

Fig. 6. Spectrum of the field transmitted through a slab of clamped electric molecules versus frequency (gigahertz).

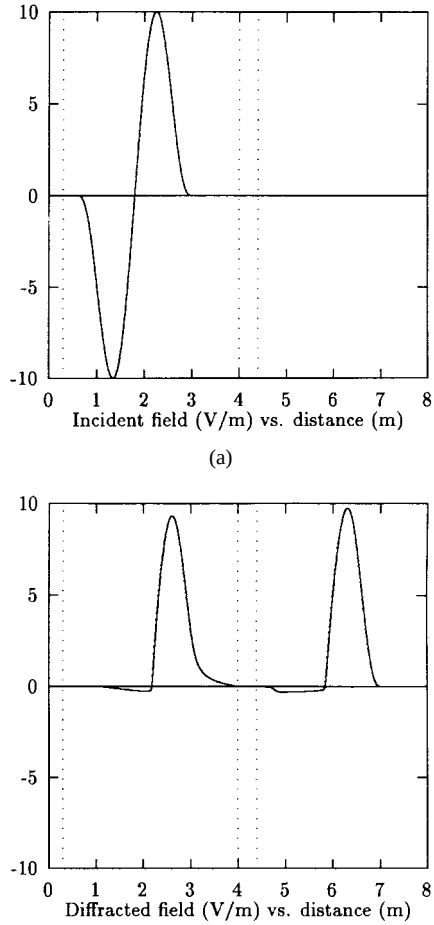

Fig. 7. A bipolar single-cycle pulsed plane wave interacts with the forward-biased clamped-molecule slab. (a) Incident electric field. (b) Reflected and transmitted electric fields.

$10.0/f_{\rm inc} = 10.0$ ns. The spatial discretization (square cells) was then set at $\Delta = 2.0$ mm $= \lambda_{\rm inc}/150$; the total length of the simulation space was 6.0 m or 3000 cells. The thickness of the slab was taken to be 1200.0 mm $= 4.0\lambda_{\rm inc}$ or 600 cells. The electric fields reflected from and transmitted through the clamped-molecule slab as obtained with our FDTD simulator are shown in Fig. 5. We can see from Fig. 5 that the shape of the field is very close to the shape of the current, i.e., the electric field is being clamped by the material. Therefore, we expected to find some low-order harmonics of the incident frequency ω_0 in its spectrum as well as a strong dc response. This is confirmed in Fig. 6, where the amplitude spectrum of the transmitted field is given.

We also considered the case where the incident field had an amplitude of 10.0 V/m to understand what other nonlinear effects might be associated with this material. We found that the clamping was more pronounced, resulting in fully rectified reflected and transmitted fields. The negative portion of the incident waveform was reflected, and the positive portion was transmitted with only minor distortions.

To test this rectification further, we considered the scattering results for a one-cycle form of the plane wave field (25) with an amplitude of 10.0 V/m incident on a 40.0-cm-thick clamped-molecule slab. The total time width of the pulse was 8.0 ns, which corresponds to a center frequency of 125 MHz ($\lambda_{\rm cf} = 2.4$ m). Thus, the slab was only $\lambda_{\rm cf}/6$ thick. Similar results were obtained with a 1.0-ns-wide pulse whose center frequency was 1.0 GHz. The lower frequency value allowed us to keep the pulsewidths and slab widths similar to the multiple-cycle case. The incident electric field is shown in Fig. 7(a), at a time before it has encountered the slab; the resulting reflected and transmitted electric fields at a time after the pulse has interacted with the slab are shown in Fig. 7(b). The dotted vertical line to the left is the total field-scattered field boundary from which the initial pulsed plane wave was launched. The second and third dotted vertical lines from the left represent the interfaces of the clamped-molecule slab. These fields are clearly appropriately rectified versions of the incident electric field.

This result was extended to the reverse diode case as well. To change the direction of the diode in the load circuit, we reversed the direction of the voltage drop across the diode and the direction of positive current through it. This led us to the following modified current equations:

$$-i(t) = I_s(e^{-\alpha v_d(t)} - 1) \tag{26}$$

$$-\frac{di}{dt} = -\alpha(-i + I_s)\frac{dv_d}{dt} \tag{27}$$

$$\frac{di}{dt} = \frac{\alpha(-i + I_s)}{1 + R\alpha(-i + I_s)}\left[\frac{l_0}{\epsilon_0}\frac{\partial H_y}{\partial z} - \left(\frac{1}{C_d} + \frac{l_0^2}{\epsilon_0 V}\right)i\right]. \tag{28}$$

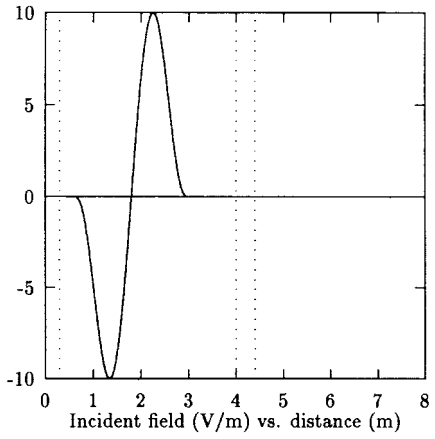

(a)

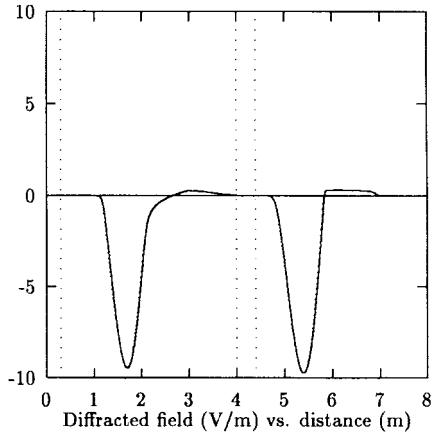

(b)

Fig. 8. A bipolar single-cycle pulsed plane wave interacts with the reverse-biased clamped-molecule slab. (a) Incident electric field. (b) Reflected and transmitted electric fields.

Our FDTD simulator was then converted to solve the system of equations defined by (22), (23), and (28). The one-cycle 10.0-V/m incident electric field is shown in Fig. 8(a) at a time before it has encountered the slab. The resulting reflected and transmitted electric fields at a time after the pulse has interacted with this reversed-diode-molecule slab are shown in Fig. 8(b). The dotted vertical line to the left is the total field-scattered field boundary from which the initial pulsed plane wave was launched. The second and third dotted vertical lines from the left represent the interfaces of the clamped-molecule slab. As expected, these fields are rectified opposite to those shown in Fig. 7.

Thus, a slab of clamped dielectric molecules could be made to convert a narrow bandwidth carrier signal into a rectified signal, i.e., a baseband broad-bandwidth signal. This is significant because standard sources will not radiate dc components into their far fields. The signal resulting from the clamped-molecule convertor would have these low-frequency components in it, as well as the carrier frequency and several higher harmonics. Such a converted waveform would be ideal for target identification applications. The low-frequency components would be able to excite the body resonances of a target, while the higher frequency components would be able to excite its fine details.

The forward- and reverse-biased clamped-molecule materials can be used in tandem to create a rectified pulse train from a single-cycle pulse. Consider two clamped-molecule slabs separated by a distance d. Let the slab closest (left slab) to the source be forward-biased, the latter (right slab) be reverse-biased. By increasing the saturation current value to $I_s = 6.0 \times 10^{-8}$ A, we found that we could cause the reverse-biased slab to be perfectly reflecting to a positive electric field pulse. For the single-cycle pulse used to create Figs. 7 and 8, we obtained the electric-field waveforms at various times, shown in Fig. 9. The vertical lines indicate the slab interfaces and total field-scattered field boundary. The distance between the slabs was $d = 3.0\ \text{m} = 10.0\lambda_{\text{inc}}$. The slabs were now taken to be $10.0\ \text{cm} = \lambda_{\text{cf}}/24$ thick. The pulse at $t = 12$ ns has interacted with the first slab and the rectified reflected and transmitted pulses have been produced. At $t = 15$ ns, the transmitted pulse has been almost totally reflected from the second slab; it has propagated further away from the second slab at $t = 18$ ns. At $t = 22$ ns, this reflected pulse begins to interact with the first slab. Since the pulse reincident on the forward-bias slab now has a smaller amplitude, some of it will penetrate through the slab and some will be reflected. This effect is shown by the electric fields at $t = 25$ ns and $t = 28$ ns.

This reflection-transmission pulse cycle will continue until there is no energy left in the cavity formed by the forward- and reverse-biased slabs. This process provides us with the means to achieve a rectified pulse train from a single-cycle incident pulse. Moreover, the distance between the individual rectified pulses will correspond to the round-trip time through the cavity. This is demonstrated in Fig. 10, which gives the reflected electric field at a point in the total field region as a function of time. The first pulse is the incident waveform, the second is the field first reflected from the forward-biased slab, and the remaining pulses are those created by the effective cavity. The small negative tail on the second pulse occurs because of the larger saturation current value. More of the negative portion of the incident pulse is not clamped by the material. The backward-biased wall acts as a perfect reflector to the positive rectified signal for the same reason, i.e., the saturation current is much larger with the opposite sign so the positively rectified signal, even though it has a small negative portion, cannot penetrate the reverse-bias slab and is reflected from it. This was confirmed by placing a perfect electric conductor wall in the same location as the first interface of the second slab; the results obtained were essentially the same as those shown in Fig. 10. The Fourier transforms of the incident pulse and reflected-field time history, excluding the incident pulse and first reflected pulse (note that with the arrangement of the two slabs, this effective time history is a train of negatively biased single half-cycle pulses), are given in Fig. 11. The spectrum of the single-cycle pulse is centered at 125 MHz as expected and has a broad bandwidth. The spectrum of the reflected-field pulse train has a dc component, and peaks at 50 MHz and at higher order multiples of the 50-MHz component. These frequency spectrum peaks all have narrow linewidths. The distance between the time-domain peaks of the rectified pulses

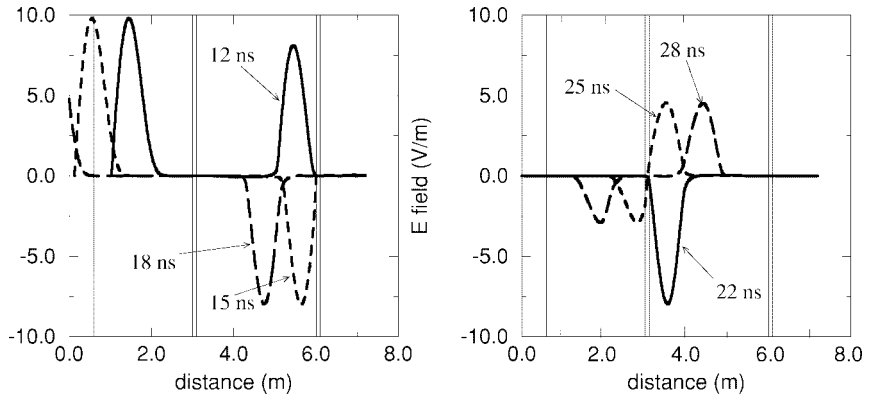

Fig. 9. The time histories of the electric fields transmitted into, trapped in, and reflected from the clamped-diode material cavity.

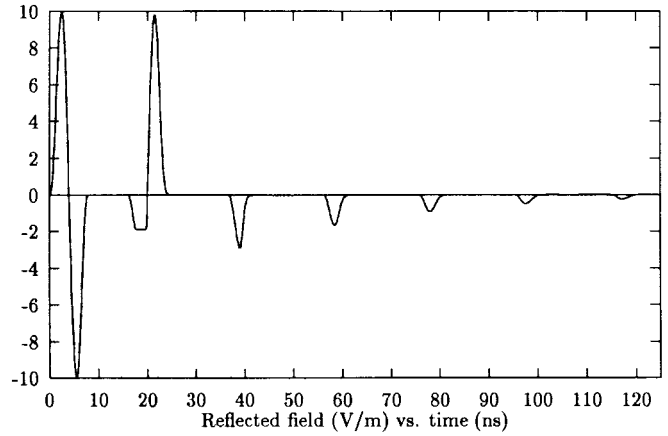

Fig. 10. The time history of the electric field in the reflected-field region of the clamped-diode material cavity.

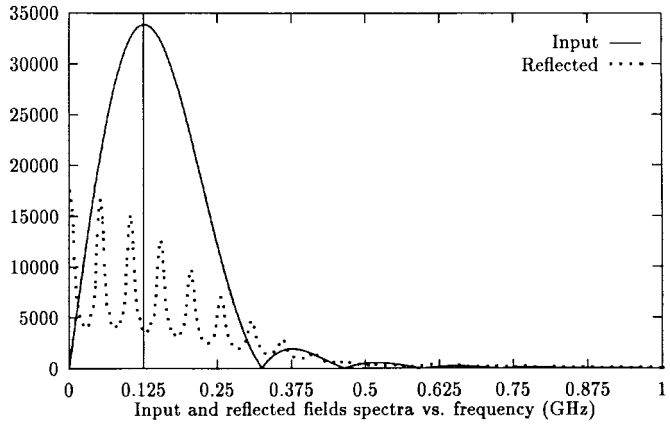

Fig. 11. Spectra of the incident electric-field pulse and of rectified reflected pulse train generated by the clamped-diode material cavity.

is $T_d = 20.0$ ns, which corresponds to the distance $cT_d = 6.0$ m, the round-trip distance between the slabs. The 20-ns separation corresponds to the 50-MHz frequency component. These results show the bandwidth of the incident pulse has been converted by the nonlinear cavity into dc and harmonic components corresponding to the cavity length.

The cavity length can be significantly shortened by introducing materials into the cavity that have nonunity permittivities and permeabilities. For example, if a tapered material with a

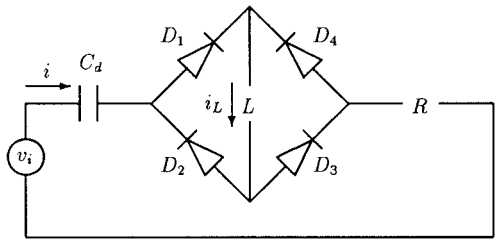

Fig. 12. Inductor-loaded diode–bridge circuit for the diode–bridge electric molecule.

relative permittivity ϵ_r and permeability μ_r that satisfy the relation $\epsilon_r = \mu_r = 1.0 + \alpha z^n$, where z is the depth into the material, then a filled clamped diode cavity of length d_{fill} will produce essentially the same rectified pulse results as the empty cavity of length d_{empty} if $\alpha = (n+1)(d_{\text{empty}} - d_{\text{fill}})/d_{\text{fill}}^{n+1}$. Extremely thin filled cavities could be realized with extremely large values of the relative permittivities and permeabilities. These conclusions have been verified with the FDTD simulator.

To achieve a transmitted pulse train with similar properties, we note that we have found that decreasing the slabs thicknesses to 2.0 cm $= \lambda_{\text{cf}}/120$ allows the fields to penetrate through the reverse-biased slab. The transmitted rectified pulse train will have its polarity opposite to that of the reflected rectified pulse train, but essentially the same magnitudes of the temporal- and frequency-domain responses. We also note that the two saturation current values considered here might be realized by using two different types of diodes or by exploiting the temperature dependence of a diode's saturation current (we note that with a common temperature model of the diode's saturation current, one can show that if $I_s = 2.0 \times 10^{-9}$ A at 300 K, then $I_s = 6.0 \times 10^{-8}$ A at 325 K).

IV. Other Nonlinear Molecules

Many other types of nonlinear molecules are possible. The only theoretical limitation seems to be the limits of the imagination of the researchers and the possibilities of coupling the appropriate differential equations to a FDTD simulator. We are currently studying a variety of more complicated load circuits having more complicated combinations of diodes and other active nonlinear devices.

An interesting example of a more complex nonlinear circuit is the one shown in Fig. 12. The load is composed of a diode bridge with an inductor load in the center of the bridge. We can see that, depending on the sign of v_i, only two diodes are forward biased at any one time: $v_i > 0$: D_1 and D_3 and $v_i < 0$: D_2 and D_4 The equations that describe the behavior of this molecule are readily obtained. Two incident voltage regimes must be considered.

If $v_i > 0$: In this case, the voltages and currents satisfy the relations

$$v_i = Ri + v_3 + v_L + v_1 + v_{C_d} \tag{29}$$

$$i = i_L = i_1 = i_3. \tag{30}$$

The currents in the forward-biased diodes are given by

$$i_1 = I_s(e^{\alpha v_1} - 1) \tag{31}$$

$$i_3 = I_s(e^{\alpha v_3} - 1). \tag{32}$$

These lead to the result that $v_1 = v_3$. Therefore, the system of equations we must solve is

$$v_3 = \frac{1}{2}(v_i - Ri - v_L - v_C) \tag{33}$$

$$i_L = I_s(e^{\alpha v_3} - 1) = i. \tag{34}$$

If $v_i < 0$: In this case, we find that $v_2 = v_4$ and the corresponding equations are

$$v_2 = \frac{1}{2}(v_C - v_L - v_i + Ri) \tag{35}$$

$$i_L = I_s(e^{\alpha v_2} - 1) = -i. \tag{36}$$

In either case, we can update the voltages with the expressions

$$v_L = L\frac{di_L}{dt} \tag{37}$$

$$\frac{dv_C}{dt} = \frac{i}{C_d}. \tag{38}$$

These systems of equations can be put into the following ordinary differential equation form:

$$\frac{di_L}{dt} = -\frac{\alpha}{2}(i_L + I_s) \cdot \left[L\frac{d^2 i_L}{dt^2} + R\frac{di_L}{dt} + \frac{i_L + I_s}{C_d} - \operatorname{sgn}(v_i)\frac{dv_i}{dt}\right] \tag{39}$$

$$i = i_L \operatorname{sgn}(v_i) \tag{40}$$

which again can be solved with a simple RK solver. For a sinusoidal voltage source, we find the behavior, shown in Fig. 13, for the current at the terminals of the dipole and its spectrum. The current is seen to be composed of alternating positive or negative clamped pulses depending on the sign of the input voltage. The corresponding spectrum now contains only the odd harmonics of the input frequency. Thus, a slab of these diode–bridge molecules would act as an odd-harmonic-generation material.

On the other hand, if the load across the bridge is another capacitance C_2 rather than an inductor, the ordinary differential equation reduces to a simpler first-order nonlinear form

$$\frac{di_{C2}}{dt} = \frac{\operatorname{sgn}(v_i)\frac{dv_i}{dt} - i_{C2}\left(\frac{1}{C_d} + \frac{1}{C_2}\right)}{R + \frac{2}{\alpha(i_{C_2} + 2I_s)}} \tag{41}$$

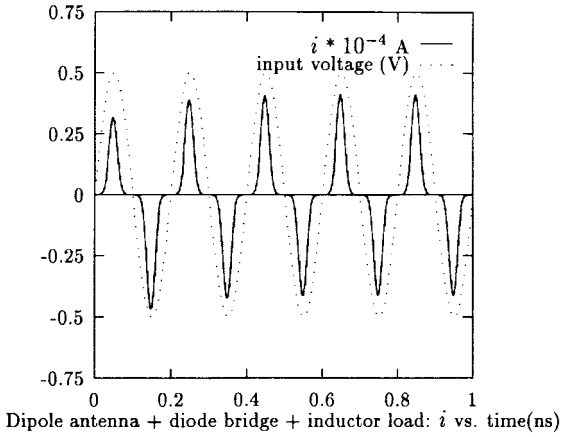

(a)

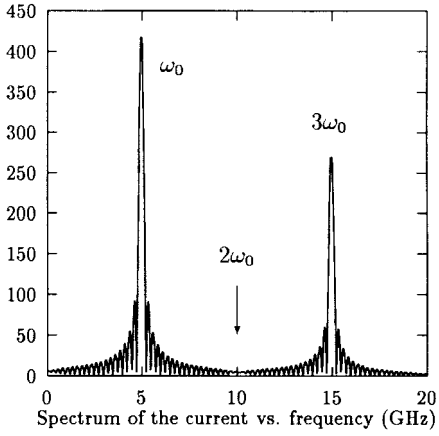

(b)

Fig. 13. The current on the dipole of the diode–bridge electric molecule and its spectrum.

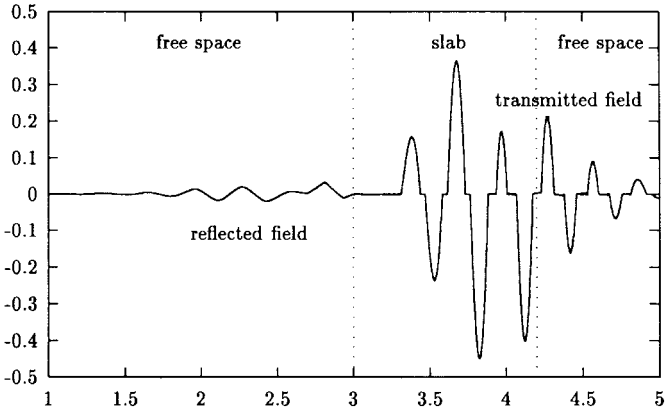

Fig. 14. Scattering from diode–bride electric molecules. Electric field (volts per meter) versus simulation region distance (meter).

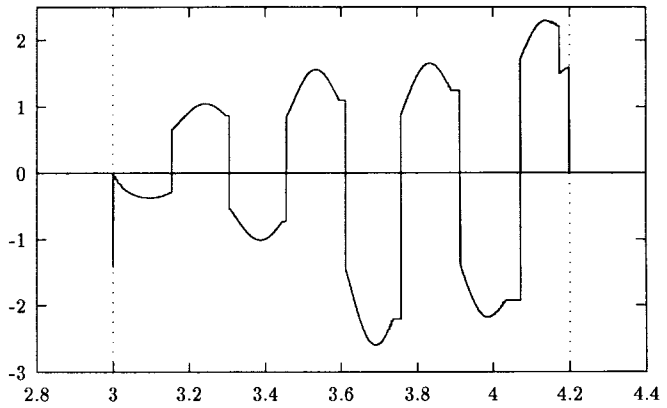

Fig. 15. The normalized current at the terminals of the diode–bride molecules (i/I_s) versus simulation region distance (meter).

where the current $i = \mathrm{sgn}(v_i)(i_{C2} + I_s)$. The results are qualitatively the same, but this auxiliary ordinary differential equation is easier to implement in the FDTD scheme. Thus, we solve (22), (23), and (41) to obtain the behavior of an electromagnetic field in a diode–bridge-molecule composite material.

For this last case, the slab parameters were modified slightly from the clamped-diode case. The half-length of the dipole was now $l_0 = 2.0$ cm and the wire diameter was $a_d = 0.18$ mm $= l_0/112$. The additional capacitor value was set to the same value as that of the dipole antenna. The electric field scattered from a slab of composite material composed of these diode–bridge molecules is plotted on Fig. 14 for the same unit amplitude incident field used in the simple clamped electric molecule case. This allows us to have either an actual capacitor in the center of the bridge or to consider the possibility to have another dipole antenna there. The latter could lead to a nonlinear bianisotropic molecule. The attenuation is stronger in this material, and the shape of the transmitted field is very similar to that of the current shown in Fig. 13. Consequently, the spectrum of the transmitted electric field has the same odd-harmonic-only properties.

Fig. 15 shows the current on the terminals of each antenna in this medium. One can see the clamping that occurs on opposite swings in the voltage in time, as well as the changes of sign spatially due to the changes in $\partial H_y/\partial z$ in the slab. The FDTD simulator accounts not only for the behavior of each molecule, but also their more intricate couplings.

V. Conclusion

In this paper, we have shown how to derive the electromagnetic properties of molecules formed by one or several small antennas connected to passive nonlinear loads. Depending on the complexity of the circuit and nonlinear elements in it, it is possible to obtain very different behaviors. It was demonstrated that a composite material formed from clamped electric molecules and excited by a narrow-bandwidth incident wave leads to a clamping, i.e., rectification, of the transmitted fields. The resulting baseband broad-bandwidth waveform may have target identification applications. It was also demonstrated that a composite material formed from diode–bridge electric molecules and excited by a narrow-bandwidth incident wave leads to transmitted fields containing odd harmonics of the incident time signal. Harmonic generation at microwave frequencies with a lightweight dielectric-based material could have a number of signal modulation and communication applications.

With any of these artificial molecules, issues pertaining to their realization obviously exist. One needs components that are smaller than the electrically small antennas under consideration to effectively integrate them together. If the antennas are approximately 1/5 of a wavelength in size or smaller to be considered electrically small, the components should be about 1/10 of a wavelength in size. Moreover, the values of the wire diameters we used in the simulations are very small even for the 1.0-GHz signals considered. These wires would require a microfabrication process to realize them, particularly with the fill-factors we considered. Furthermore, the component values need to be stable over large bandwidths if ultrawide-bandwidth applications are desired. This may not be much of an issue with the capacitors and resistors, but it is with any inductors. Several efforts are in progress to experimentally investigate the passive linear load molecules. We anticipate similar interest in these nonlinear molecules and their potential applications.

We are currently studying molecules formed with active nonlinear loads so that more complex interactions and output waveforms can be achieved. Since these devices are active, their currents are larger and circumvent the wire thickness issue. However, the more complex the circuit, the more volume it will require and the fill-factor may remain an issue. Nonetheless, these active nonlinear devices provide significant enhancements to the possible molecular circuits. Operational amplifier-based circuits can lead to amplifiers, oscillators, integrators, differentiators, frequency dividers, or frequency multipliers. Molecules can be designed to utilize these behaviors. The results of our current investigations into these active materials will be presented elsewhere.

References

[1] I. V. Lindell, A. H. Sihvola, S. A. Tretyakov, and A. J. Vitanen, *Electromagnetic Waves in Chiral and Bi-Isotropic Media*. Norwood, MA: Artech House, 1994, pp. 8–14.

[2] F. Mariotte, S. A. Tretyakov, and B. Sauviac, "Isotropic chiral composite modeling: Comparison between analytical, numerical, and experimental results," *Microwave Opt. Technol. Lett.*, vol. 7, no. 18, pp. 861–864, Dec. 1994.

[3] F. Mariotte and J.-P. Parneix, Eds., *Proc. Chiral'94 Workshop, 3rd Int. Workshop Chiral, Bi-isotropic, Bi-anisotropic Media*, Perigueux France, May 18–20, 1994.

[4] R. W. Ziolkowski and F. Auzanneau, "Passive artificial molecule realizations of dielectric materials," *J. Appl. Phys.*, vol. 82, no. 7, pp. 3195–3198, Oct. 1997.

[5] ——, "Artificial molecule realizations of a magnetic wall," *J. Appl. Phys.*, vol. 82, no. 7, pp. 3192–3194, Oct. 1997.

[6] F. Auzanneau and R. W. Ziolkowski, "Theoretical study of synthetic bianisotropic materials," *J. Electromagn. Waves Applicat.*, vol. 12, no. 3, pp. 353–370, Dec. 1997.

[7] ——, "Étude théorique de matériaux bianisotropes synthétiques contrôlables," *J. Phys. III*, vol. 7, pp. 2405–2418, Dec. 1997.

[8] R. W. Ziolkowski and F. Auzanneau, "The design of Maxwellian smart skins," in *Proc. 13th ACES Symp.*, Monterey CA, Mar. 17–21, 1997, pp. 98–103.

[9] K. E. Oughstun and G. C. Sherman, *Electromagnetic Pulse Propagation in Causal Dielectrics*. Berlin, Germany: Springer-Verlag, 1994.

[10] R. W. Ziolkowski, "The design of Maxwellian absorbers for numerical boundary conditions and for practical applications using engineered artificial materials," *IEEE Trans. Antennas Propagat.*, vol. 45, pp. 656–671, Apr. 1997.
[11] ———, "Time-derivative Lorentz materials and their utilization as electromagnetic absorbers," *Phys. Rev. E*, vol. 55, no. 6, pp. 7696–7703, June 1997.
[12] B. Toland, J. Lin, B. Houshmand, and T. Itoh, "FDTD analysis of an active antenna," *IEEE Microwave Guided Wave Lett.*, vol. 3, pp. 423–425, Nov. 1993.
[13] B. Toland and T. Itoh, "Modeling of nonlinear active regions with the FDTD method," *IEEE Microwave Guided Wave Lett.*, vol. 3, pp. 333–335, Sept. 1993.
[14] C.-N. Kuo, V. A. Thomas, S. T. Chew, B. Houshmand, and T. Itoh, "Small signal analysis of active circuits using FDTD algorithm," *IEEE Microwave Guided Wave Lett.*, vol. 5, pp. 216–218, July 1995.
[15] C.-N. R.-B. Wu, Kuo, B. Houshmand, and T. Itoh, "Modeling of microwave active devices using the FDTD analysis based on the voltage-source approach," *IEEE Microwave Guided Wave Lett.*, vol. 6, pp. 199–201, May 1996.
[16] C.-N. Kuo, B. Houshmand, and T. Itoh, "Full-wave analysis of packaged microwave circuits with active and nonlinear devices: An FDTD approach," *IEEE Trans. Microwave Theory Tech.*, vol. 45, pp. 819–826, May 1997.
[17] M. Piket-May, A. Taflove, and J. Baron, "FD-TD modeling of digital signal propagation in 3-D circuits with passive and active loads," *IEEE Trans. Microwave Theory Tech.*, vol. 42, pp. 1514–1523, Aug. 1994.
[18] V. A. Thomas, M. E. Jones, M. Piket-May, A. Taflove, and E. Harrigan, "The use of SPICE lumped circuits as sub-grid models for FDTD analysis," *IEEE Microwave Guided Wave Lett.*, vol. 4, pp. 141–143, May 1994.
[19] M. A. Alsunaidi, S. M. S. Imtiaz, and S. M. El-Ghazaly, "Electromagnetic wave effects on microwave transistors using a full-wave time-domain model," *IEEE Trans. Microwave Theory Tech.*, vol. 44, pp. 799–808, June 1996.
[20] W. Sui, D. A. Christensen, and C. H. Durney, "Extending the two-dimensional FD-TD method to hybrid electromagnetic systems with active and passive lumped elements," *IEEE Trans. Microwave Theory Tech.*, vol. 40, pp. 724–730, Apr. 1992.
[21] R. F. Churchhouse, Ed., *Handbook of Applicable Mathematics, Vol III: Numerical Methods*. New York: Wiley, 1981, pp. 321–325.
[22] I. V. Lindell, A. H. Sihvola, S. A. Tretyakov, and A. J. Vitanen, *Electromagnetic Waves in Chiral and Bi-Isotropic Media*. Norwood, MA: Artech House, 1994, pp. 208–209.
[23] R. J. Gehr and R. W. Boyd, "Optical properties of nanostructured optical materials," *Chem. Mater.*, vol. 8, no. 8, pp. 1807–1819, 1996.

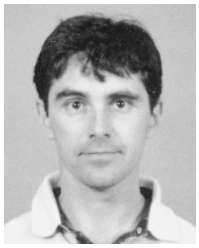

Fabrice Auzanneau received the diploma degree from the Ecole Nationale Superieure de l'Aeronautique et de l'Espace, Toulouse, France, in 1987.

Since 1988, he has been with the CEA CESTA Laboratory, Le Barp, France, where he is currently an Engineer, involved with topics related to electromagnetism and stealth. From 1996 to 1997, he was a Visiting Scholar with the Department of Electrical and Computer Engineering, University of Arizona, Tucson.

Richard W. Ziolkowski (M'87–SM'91–F'94) received the Sc.B. degree in physics *magna cum laude* with honors from Brown University, Providence, RI, in 1974, and the M.S. and Ph.D. degrees in physics from the University of Illinois at Urbana-Champaign, in 1975 and 1980, respectively.

From 1981 to 1990, he was a member of the Engineering Research Division, Lawrence Livermore National Laboratory, where, from 1984 to 1990, he served as the Leader of the Computational Electronics and Electromagnetics Thrust Area for the Engineering Directorate. In 1990, he joined the Department of Electrical and Computer Engineering, University of Arizona, Tempe, as an Associate Professor, and was promoted to Full Professor in 1996. His research interests include the application of new mathematical and numerical methods to linear and nonlinear problems dealing with the interaction of acoustic and electromagnetic waves with realistic materials and structures.

Prof. Ziolkowski is a member of Tau Beta Pi, Sigma Xi, Phi Kappa Phi, American Physical Society, Optical Society of America, Acoustical Society of America, and Commission B (Fields and Waves) of URSI. He is an associate editor for the IEEE TRANSACTIONS ON ANTENNAS AND PROPAGATION. He served as the vice chairman of the 1989 IEEE/AP-S and URSI Symposiums, San Jose, CA. He was the technical program chairperson for the 1998 IEEE Conference on Electromagnetic Field Computation, Tucson, AZ. He was the secretary for the US URSI Commission B from 1993 to 1996, and is currently serving as the chairperson of the Technical Activities Committee. He was awarded the Tau Beta Pi Professor of the Year Award in 1993 and the IEEE and Eta Kappa Nu Outstanding Teaching Award in 1993 and 1998.